A&A 578, A71 (2015)
DOI: 10.1051/0004-6361/201526112

Astronomy & Astrophysics

Unveiling the population of orphan γ-ray bursts

G. Ghirlanda[1], R. Salvaterra[2], S. Campana[1], S. D. Vergani[3,1], J. Japelj[4], M. G. Bernardini[1], D. Burlon[5,6], P. D'Avanzo[1], A. Melandri[1], A. Gomboc[4], F. Nappo[7,1], R. Paladini[8], A. Pescalli[7,1], O. S. Salafia[9,1], and G. Tagliaferri[1]

[1] INAF–Osservatorio Astronomico di Brera, via E. Bianchi 46, 23807 Merate, Italy
e-mail: giancarlo.ghirlanda@brera.inaf.it
[2] INAF–IASF Milano, via E. Bassini 15, 20133 Milano, Italy
[3] GEPI, Observatoire de Paris, CNRS, Univ. Paris Diderot, 5 place Jules Janssen, 92190 Meudon, France
[4] Faculty of Mathematics and Physics, University of Ljubljana, Jadranska 19, 1000 Ljubljana, Slovenia
[5] Sydney Institute for Astronomy, School of Physics, The University of Sydney, NSW 2006, Australia
[6] ARC Centre of Excellence for All-sky Astrophysics (CAASTRO), Camberra, ACT 2611, Australia
[7] Universitá degli Studi dell'Insubria, via Valleggio 11, 22100 Como, Italy
[8] NASA Herschel Science Center, California Institute of Technology, 1200, East California Boulevard, Pasadena, CA 91125, USA
[9] Dipartimento di Fisica G. Occhialini, Universitá di Milano Bicocca, Piazza della Scienza 3, 20126 Milano, Italy

Received 17 March 2015 / Accepted 7 April 2015

ABSTRACT

Gamma-ray bursts (GRBs) are detectable in the γ-ray band if their jets are oriented toward the observer. However, for each GRB with a typical $\theta_{\rm jet}$, there should be $\sim 2/\theta_{\rm jet}^2$ bursts whose emission cone is oriented elsewhere in space. These off-axis bursts can eventually be detected when, due to the deceleration of their relativistic jets, the beaming angle becomes comparable to the viewing angle. Orphan afterglows (OAs) should outnumber the current population of bursts detected in the γ-ray band even if they have not been conclusively observed so far at any frequency. We compute the expected flux of the population of orphan afterglows in the mm, optical, and X-ray bands through a population synthesis code of GRBs and the standard afterglow emission model. We estimate the detection rate of OAs with ongoing and forthcoming surveys. The average duration of OAs as transients above a given limiting flux is derived and described with analytical expressions: in general OAs should appear as daily transients in optical surveys and as monthly/yearly transients in the mm/radio band. We find that $\sim$2 OA yr^{-1} could already be detected by *Gaia* and up to 20 OA yr^{-1} could be observed by the ZTF survey. A larger number of 50 OA yr^{-1} should be detected by LSST in the optical band. For the X–ray band, $\sim$26 OA yr^{-1} could be detected by the eROSITA. For the large population of OA detectable by LSST, the X-ray and optical follow up of the light curve (for the brightest cases) and/or the extensive follow up of their emission in the mm and radio band could be the key to disentangling their GRB nature from other extragalactic transients of comparable flux density.

Key words. gamma-ray burst: general – relativistic processes

1. Introduction

Gamma-ray bursts (GRBs) are cosmological sources that signpost the birth of stellar mass black holes or the most intense magnetic fields harbored by compact objects (magnetars). They are detected as short, highly variable, flashes of γ-rays (prompt emission) with duration that is typically in the range 0.1 to 1000 s followed by a smoothly decaying long-lived emission at X-ray, optical, and radio frequencies (the afterglow – Costa et al. 1997; van Paradijs et al. 1997). In the standard fireball model the prompt emission is interpreted as due to internal dissipation (either through relativistic shocks or magnetic reconnection), whereas the afterglow is produced by the deceleration of the relativistic outflow by the circumburst interstellar medium.

Theoretical arguments (e.g., Sari & Piran 1999) and direct observational evidence (e.g., Molinari et al. 2007) suggest that the outflow of GRBs is relativistic with typical bulk Lorentz factors $\Gamma_0 \sim 10^{2-3}$. The most luminous and energetic GRBs seem to have larger Γ_0 (e.g., Liang et al. 2010; Ghirlanda et al. 2012). Another key property of GRBs is the presence of a jet. Invoked to reduce the otherwise huge isotropic equivalent energies by a factor proportional to $\theta_{\rm jet}^2$ (i.e., the jet half-opening angle), jet angles have been estimated in a few tens of GRBs from the steepening of the optical and/or X-ray light curve a few days after the prompt emission. This steepening is interpreted as the time when, because of the deceleration of the outflow, the relativistic beaming $\propto 1/\Gamma$ equals the geometric collimation $\theta_{\rm jet}$. Modeling of the outflow dynamics (Blandford & McKee 1976) allows us to infer the GRB jet opening angle $\theta_{\rm jet}$ (Rhoads 1999). The collimation corrected energies were found to be distributed around 10^{51} erg (Frail et al. 2001) with a smaller dispersion with respect to that of the isotropic equivalent energies (but see Gehrels et al. 2009).

The satellites/instruments deputed to the detection of GRBs observed hundreds/thousands of GRBs at an average rate of $\sim$0.3 day^{-1}. However, if GRBs have a jet with energy and bulk Lorentz factors that are constant within the jet as a function of the angle from its axis and Γ_0 (pointed radially as the expansion of the outflow within the jet) is relatively large (typically a few hundred), we can only detect those bursts whose jet is pointing at the Earth. Indeed, since the highly relativistic motion results in a strong forward beaming of the emitted radiation, the flux directed at the Earth is dramatically reduced when $\theta_{\rm view} > \theta_{\rm jet}$, where $\theta_{\rm view}$ is the viewing angle between the jet axis and the line of sight. These events, which are the most numerous due to the jet orientation probability being $\propto \sin\theta_{\rm view}$,

go undetected as prompt GRBs. During the afterglow, however, the bulk Lorentz factor decreases with time, as the outflow is decelerated by the external medium. There is a characteristic timescale when the relativistic beaming $\propto 1/\Gamma$ equals the observer viewing angle $\theta_{\rm view}$ and the (afterglow) radiation can be seen. These events, missing the prompt emission but detected as afterglows, are called orphan afterglows (OAs) and, for typical opening angles of GRBs of a few degrees, e.g., $\theta_{\rm jet} \sim 0.1$ rad, they should outnumber the population of GRBs (by a factor $\propto (1-\cos\theta_{\rm jet})^{-1} \sim 200$).

Therefore, OAs should be detected as transients but their association with GRBs is made difficult because of the lack of prompt high-energy emission. Despite specific studies designed to search for OAs in X-ray surveys (Grindlay 1999; Greiner et al. 2000), in optical surveys (Vreeswijk 2002; Rau et al. 2006; Malacrino et al. 2007; Rau et al. 2007), and in the radio band (Levinson et al. 2002; Gal-Yam et al. 2006; Bannister et al. 2011; Bell et al. 2011; Bower & Saul 2011; Croft et al. 2010; Frail et al. 2012; Carilli et al. 2003; Matsumura et al. 2009; Lazio et al. 2010), no OA have been conclusively detected so far.

Nondetections of OA are in agreement with current theoretical predictions (Totani & Panaitescu 2002; Nakar et al. 2002; Zou et al. 2007; Rossi et al. 2008; Metzger et al. 2015). However, these works either extrapolated the properties of a few known GRB afterglows to the orphans (e.g., Totani & Panaitescu 2002) or assumed basic prescriptions for the known GRB population properties or for the afterglow emission model. We recently developed a population synthesis code (Ghirlanda et al. 2013a) which, coupled with the most detailed model for the afterglow emission (van Eerten et al. 2012), allows us to predict the properties of the population of OAs (Ghirlanda et al. 2014), reproducing a large set of observed properties of the population of the "Earth–pointed" GRBs. So far, we considered the radio band predicting that the Square Kilometer Array (SKA), reaching the μJy flux limit, could see up to ~0.2–1.5 OA deg^{-2} yr^{-1} (Ghirlanda et al. 2014). Alternatively, the nondetection of OA could be due to the structure of the jet (Rossi et al. 2008; Salafia et al. 2015).

We are entering the era of large synoptic surveys, which will monitor large portions of the (if not the whole) sky with unprecedented sensitivities. Orphan afterglows are potentially in the list of transients that these surveys will detect, but specific predictions on the rate depend on the true rate of the population of OAs (and their duration) and on the survey characteristics (area of the sky covered, timescales, limiting flux). Here we derive the flux distribution of OAs in the X-ray, optical, and mm band (Sect. 3) based on our recent population synthesis code (Sect. 2). We also study the average duration of the population of OAs as a function of the survey limiting flux (Sect. 3). We compare the flux distributions with current limits of OAs in these bands and make predictions for ongoing and forthcoming surveys (Sect. 4). Standard cosmological parameters ($h = \Omega_\Lambda = 0.7$) for a flat Universe are adopted throughout the paper.

2. Orphan afterglow emission

The only difference between OAs and GRBs is the orientation of their jets with respect to the line of sight. This allows us to use all the known properties of GRBs detected so far in the γ-ray band and with well-studied afterglow emission to infer the emission characteristics of OAs. In particular, OAs are normal GRBs with their jet oriented so that $\theta_{\rm view} > \theta_{\rm jet}$.

To predict the properties of OAs, first we need a model describing the entire population of GRBs distributed in the Universe. We use the population code developed recently in Ghirlanda et al. (2013a, G13 hereafter) and extended in Ghirlanda et al. (2014, G14 hereafter), called PSYCHE (Population SYnthesis Code and Hydrodynamic Emission model). The PSYCHE model generates bursts with a redshift z (assigned following the GRB formation rate; Hopkins & Beacom 2008), a jet opening angle $\theta_{\rm jet}$, and a bulk Lorentz factor Γ_0. The latter two parameters are drawn from two lognormal distributions with median values 5.7° and 90, respectively. We obtained these distributions (G13) to reproduce: (a) the $E_{\rm p}-E_{\rm iso}$ correlation of a complete (flux limited) sample of *Swift* bursts (Salvaterra et al. 2012; Nava et al. 2012); (b) the flux distribution of GRBs detected by BATSE and GBM/*Fermi*; (c) the detection rate of GRBs by *Swift*, *Fermi*, and BATSE. The isotropic equivalent energy $E_{\rm iso}$ and rest-frame peak energy $E_{\rm p}$ are obtained, once $\theta_{\rm jet}$ and Γ_0 are extracted, assuming a universal comoving frame that is collimation corrected and energetic (see G13 for details)[1].

Bursts are then assigned a viewing angle $\theta_{\rm view}$, according to the $\sin\theta_{\rm view}$ probability distribution, representing the orientation of the jet with respect to the line of sight. Within the GRB population simulated by PSYCHE, there are bursts that can be detected as γ-ray events because $\theta_{\rm view} \le \theta_{\rm jet}$ and those that that can be detected as OAs because $\theta_{\rm view} > \theta_{\rm jet}$. The latter type of bursts are the subject of this work.

In general, since we only see the afterglow for highly relativistic GRBs seen off-axis (Sect. 1), we need to simulate the afterglow emission for each burst. To this aim, PSYCHE implements the numerical code *BOXFIT* (van Eerten & MacFadyen 2011, van Eerten et al. 2012, VE12 hereafter), which is based on numerical 2D simulations of the jet dynamics and assumes synchrotron emission from shock accelerated electrons as the radiation mechanisms of the afterglow phase. The VE12 code considers GRBs with a constant circumburst density. In this standard afterglow model, the external shock emission depends on a set of micro-physical parameters: the index p of the energy distribution of the shock accelerated electrons, the fraction of the dissipated energy distributed to electrons $\epsilon_{\rm e}$ and to the magnetic field $\epsilon_{\rm B}$. Finally, the value of the density n for the circumburst medium, is assigned. These are the free parameters determining the afterglow emission of each simulated burst.

2.1. Setting the microphysical shock parameters

Distributions of the microphysical shock parameters (p, $\epsilon_{\rm e}$, $\epsilon_{\rm B}$) are poorly constrained directly from the observations. Dense multiwavelength sampling of the afterglow light curve from early times to days after the burst explosion is available for a limited number of bursts. Panaitescu & Kumar (2000) first derived the values of these parameters through modeling the afterglow light curves of 10 GRBs in the pre-*Swift* era. The same pre-*Swift* bursts were used to derive the properties of OAs (Totani & Panaitescu 2002). However, *Swift* follow up in the X-ray band and optical monitoring campaigns have shown in recent years that afterglow emission can be very different from burst to burst. The X-ray and optical luminosities at 0.5 days after the burst have proven (e.g., D'Avanzo et al. 2012; Melandri et al. 2014) to

[1] The distribution of $\theta_{\rm jet}$ and Γ_0 are derived self-consistently in G13 to reproduce the γ-ray properties of GRBs. It is shown in G13 that even when the assumed values of the comoving frame energetics are changed by a factor of 10, the two inferred distributions are modified accordingly so that the population of GRBs has similar characteristics in terms of energetics and opening angles.

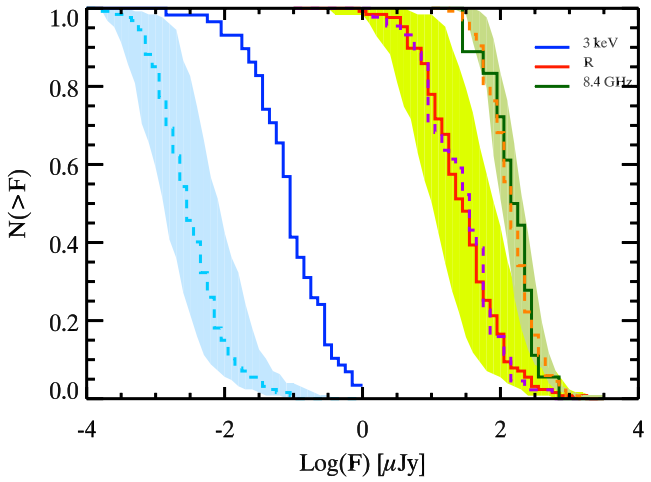

Fig. 1. Flux density cumulative distributions in the optical (R , solid red line), X-ray (at 3 keV, solid blue line) computed at 11 h after the start of the GRB emission for the BAT6 *Swift* complete sample (adapted from Melandri et al. 2014; and D'Avanzo et al. 2012, for the optical and X-ray band, respectively). The radio (at 8.4 GHz – solid green line) is from Ghirlanda et al. (2013b), also for the BAT6 sample. The results of the population synthesis code with $p = 2.3, \epsilon_e = 0.02$ and $\epsilon_B = 0.008$ are shown with the dashed lines. The shaded regions represent, for each band, the results obtained with $(p, \epsilon_e, \epsilon_B) = (2.3, 0.01, 0.001)$ for the lower boundary and $(p, \epsilon_e, \epsilon_B) = (2.3, 0.05, 0.01)$ for the upper boundary. The X-ray and R band fluxes of the *Swift* BAT6 sample (solid blue and red line respectively) have been corrected for absorption (D'Avanzo et al. 2012; Campana et al. 2012) and for dust extinction (Melandri et al. 2014; Covino et al. 2013), respectively.

be more dispersed than initially found based on a limited number of events. Moreover, a possible different origin of the X-ray and optical emission, with the latter being more genuinely afterglow, has been proposed (Ghisellini et al. 2009).

We aim to estimate the flux level of the population of OAs as a whole to compare it with the limits of current and future surveys in different bands. To this aim, we can use average values of the microphysical parameters (p, ϵ_e, ϵ_B) for the entire simulated GRB population. To assign these values, we consider the observed flux of the afterglow of the GRBs composing the complete *Swift* sample (BAT6 – Salvaterra et al. 2012). This is a flux limited sample of GRBs and it turns out to have a high level of completeness in redshift (97%). Therefore, no bias induced by the redshift estimate should be affecting the sample. Similarly, the high flux cut ensures that our sample is free from any threshold bias related to the GRB detector (BAT on board *Swift* in this case). Figure 1 shows the cumulative distribution of the optical flux (at 12 h after the burst) of the BAT6 sample (red solid line, adapted from Melandri et al. 2014), the cumulative distribution of the X-ray flux (at 3 keV and at 11 h) of the BAT6 (blue solid line, adapted from D'Avanzo et al. 2012), and the cumulative distribution of the radio flux (at 8.4 GHz between 1 and 6 days) of the BAT6 (green solid line, adapted from Ghirlanda et al. 2013a). These are the observed distributions we aim to reproduce assigning to the simulated GRB population a set of values for the microphysical parameters (p, ϵ_e, ϵ_B).

Since the BAT6 sample contains GRBs detected by *Swift* in the γ-ray band, we work on the simulated population of GRBs with $\theta_{view} \leq \theta_{jet}$. We select among this population the bright events with the same flux cut adopted for the BAT6, i.e., bursts with a peak flux larger than 2.6 ph cm^{-2} s^{-1} integrated in the 15−150 keV energy band. We assume that the circumburst density n is distributed uniformly between 0.1 and 30 cm^{-3} (also in this case we make this choice to reproduce the BAT6 optical and radio flux distributions, Fig. 1) and assign to each simulated burst a value of n randomly extracted from a uniform distribution within this range. We keep the other three parameters (p, ϵ_e, ϵ_B) fixed. We obtain the fiducial values for these three parameters by reproducing the flux distributions of the BAT6 sample shown with the solid lines in Fig. 1 at three different frequencies. With $p = 2.3$, $\epsilon_e = 0.02$ and $\epsilon_B = 0.008$ (as already discussed in Ghirlanda et al. 2013a, 2014), we obtain for the simulated population of GRBs cumulative flux distributions (dashed lines in Fig. 1), which nicely match the radio and optical flux distributions (solid lines in Fig. 1) of the real GRBs of the BAT6 sample. If we assume lower/higher values for ϵ_e and ϵ_B, we obtain lower/higher fluxes in both bands (solid shaded regions in Fig. 1).

In Fig. 1 (solid blue line), the X-ray flux cumulative distribution at 3 keV computed at 11 h (from D'Avanzo et al. 2012) is also shown. That the microphysical parameter values that reproduce the optical and radio fluxes underestimate the X-ray flux by more than one order of magnitude. This is not unexpected since the fact that X-ray emission of GRBs could be dominated at early times (typically up to half a day after the explosion) by an extra component, which is apparently unrelated to the standard afterglow forward shock emission (e.g., Ghisellini et al. 2009; D'Avanzo et al. 2012), has already been discussed in the literature.

Therefore, we assume the microphysical parameters values that reproduce the optical and radio flux distribution of a flux limited sample of real bursts.

3. Results

Following G14, we consider the time when the OA flux reaches its peak (Eq. (3) in G14) and calculate the OA flux at this time of the peak. The light curve of the OA starts to rise when $\Gamma \sim 1/\sin(\theta_{view} - \theta_{jet})$ and peaks around the time when the entire jet is visible, i.e., $\Gamma \sim 1/\sin(\theta_{view} + \theta_{jet})$. The OA flux after this time follows the same light curve that an observer would see with a line of sight within the jet opening angle. Therefore, the peak time corresponds to the maximum observed flux from the OA. According to our simulations, the time when the OA peaks, which depends on the burst parameters and on the viewing angle, has a broad distribution with a typical value of few hundred days after the GRB (note that this reference is purely theoretical, since the GRB start time is missed in the real case of an OA).

3.1. Orphan afterglows flux density

The cumulative peak flux density distributions of OAs are shown in Fig. 2. The X-ray flux density is computed at 3 keV where the photoelectric absorption by metals in the Galaxy and host galaxy is negligible (Campana et al. 2012). For the optical R flux density, we assume an A_V according to the distribution obtained by the analysis of the BAT6 sample (Covino et al. 2013). This is an asymmetric distribution of A_V peaking <0.5 mag and extending, in less than 10% of the cases, to values higher than 1–2 mag. This assumption is based on the A_V measured in bursts observed within their jet opening angle (i.e., close to the jet axis). Eventually, dust destruction by the GRB X-ray/UV flash could reduce the optical absorption close to the line of sight (Perna et al. 2003). The OAs, observed at large viewing angles, could therefore have a larger A_V than we assume. Overall, this effect would further reduce the optical fluxes of OAs observed at large

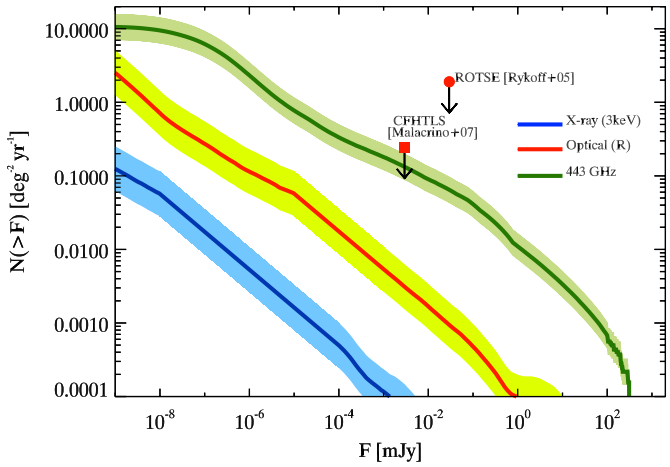

Fig. 2. Cumulative flux density distribution of OAs at three characteristic frequencies: R band for the optical (red line), 3 keV for the X-ray (blue line), and 443 GHz for the mm band (green line is representative of ALMA frequency range). Upper limits of past searches of OAs in the optical band are shown by the red symbols (to be compared with the red solid line). The optical R flux distribution is representative of the OAs at $z \leq 4.5$ because, at higher redshift, their R band flux suffers from Lyα suppression. An optical extinction (according to the distribution of Covino et al. 2013) has been applied to the optical fluxes.

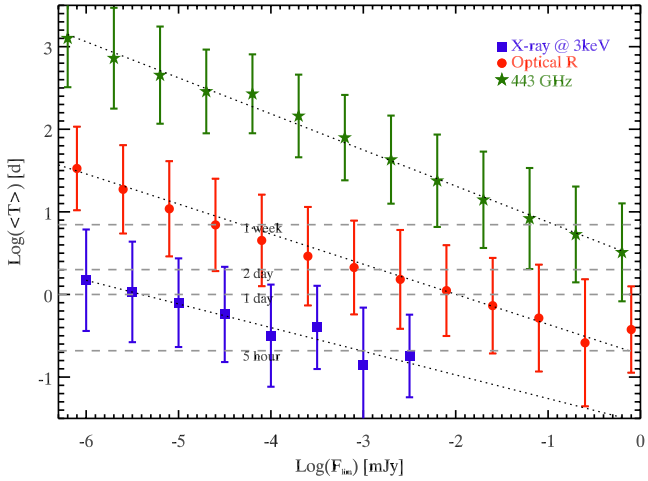

Fig. 3. Average duration of the simulated population of OAs with flux above the corresponding x-axis value. The bars represent the 1σ scatter around the average. Typical timescales are shown by the dashed horizontal lines (as labeled). Linear fits are shown by the dotted lines. Fit parameters are reported in Table 1.

Table 1. Parameters of the linear fits to the average duration of OAs above flux threshold (Fig. 3).

Band	m	q
X-ray (3 keV)	–0.28	–1.54
R (7000 Å)	–0.36	–0.72
443 GHz	–0.44	0.44

Notes. Fits parameters of the formula: $\log(\langle T\rangle_{\rm days}) = q + m\log(F_{\rm lim,mJy})$.

viewing angles and consequently reduce the predicted rates of OAs detectable in optical surveys. For the optical, we only consider OAs at $z < 4.5$ since we expect that the optical emission is fully absorbed by the Lyα absorption at higher redshifts. Also shown in Fig. 2 are the range of variation of the flux density distributions obtained by varying the microphysical parameters (as described in Sect. 2).

All the flux density distributions shown in Fig. 2 represent the flux at the time when the OA reaches its maximum emission. On average, OA should reach its maximum flux hundreds of days after the burst. At these times the afterglow emission spectrum peaks at relatively low frequencies (in the mm and radio band). This accounts for the relative normalizations of the flux cumulative distributions at different frequencies in Fig. 2. The three curves, however, converge at very low fluxes (not shown in Fig. 2 for clarity) to the total rate of OAs, which is set by the normalization of the population synthesis code to the rate of GRBs detected in the γ-ray band by *Swift*, BATSE, and *Fermi* (G13). This can be already seen in the 443 GHz curve of Fig. 2 and corresponds to 10 OA deg^{-2} yr^{-1}.

3.2. Timescales of orphan afterglows

Surveys can detect orphan afterglows as transient events when the OA flux is above the survey limiting flux. The latter, therefore, determines the rate of detectable OAs. The survey limiting flux, however, also determines the OA characteristic duration $\langle T\rangle$. At a fixed frequency, the deeper the survey, the longer the duration of OA above the survey limiting flux. We define $\langle T\rangle$ as the time interval during which the OA flux is larger than the survey flux limit $F_{\rm lim}$. Figure 3 shows the average duration of OA above $F_{\rm lim}$ for the three frequencies we consider. In general, given the typical flux limits of optical and X-ray surveys (see also Sect. 4), OAs will appear as daily transients. At GHz frequencies, they will instead be much slower transients with duration of even tens to hundreds of days (see also Ghirlanda et al. 2014). This timescale represents the duration of the OA above a given survey limit and it is only due to the instrumental limit. This should not be confused with the timescale of the peak of the OA with respect to the GRB, which is due to the combination of burst geometry (opening angle and viewing angle) and hydrodynamics (i.e., the deceleration of the fireball, which is mainly set by its kinetic energy, initial bulk Lorentz factor, and circumburst density). In general, the distribution of the time of the peak of the OA is centered around a few hundred days. However, at these times the optical emission of OA is extremely faint, so that any conceivable optical survey (also the deepest to be performed in the future) will detect those OAs that peak at relatively early times, i.e., between 1 and 10 days after the trigger, which are the brightest within the population.

Figure 3 shows that, at any frequency, the OA duration $\langle T\rangle$ increases as the survey limit deepens (i.e., with decreasing survey limiting flux $F_{\rm lim}$). Table 1 shows the parameters (slope m and normalization q) of the linear fit (dotted lines in Fig. 3) to the data shown in Fig. 3 for the three characteristic frequencies.

4. Orphan afterglows detection rate

In this section, we compare our results with past searches for OAs in the optical and X-ray band and show specific predictions for ongoing or planned surveys in these bands. We also consider forthcoming large projects like the Large Synoptic Sky Telescope (LSST) and the extended ROentgen Survey with the Imaging Telescope Array (eROSITA), which will conduct almost all sky surveys in the optical and X-ray bands, respectively. For the radio band, Ghirlanda et al. (2014) showed that the OA rates are consistent with the (upper) limits of past radio surveys, which did not detect any credible orphan afterglow.

Forthcoming radio surveys like the VAST/ASKAP at 1.4 GHz or the MeerKAT or EVLA at 8.4 GHz could detect 3×10^{-3} and 3×10^{-1} OA deg^{-2} yr^{-1}, respectively. The deeper SKA survey, reaching the μJy flux limit, could detect up to 0.2–1.5 OA deg^{-2} yr^{-1} (Ghirlanda et al. 2014). Here we report the predictions for optical and X-ray surveys.

4.1. Optical surveys

Among past searches for orphan afterglows in the optical, Rykoff et al. (2005) used the Robotic Optical Transients Search Experiment III (ROTSE–III). Over a period of 1.5 year, they identified no credible GRB afterglow. They place a 95% upper limit on the OA rate of 1.9 deg^{-2} yr^{-1} at $R = 20$. The Deep Lensing Survey (DLS; Becker et al. 2004) provides a (less constraining) limit of 5.2 deg^{-2} day^{-1} for transients with typical duration of a few ksec and $19.5 < R < 23.4$. Malacrino et al. (2007) obtained a more stringent upper limit from the CFHTLS Very Wide survey: excluding that the three transient they find are GRBs (Malacrino et al. 2007), an upper limit of 0.24 deg^{-2} yr^{-1} down to $R = 23$ can be placed. The ROTSE–III and CFHTLS limits are shown in Fig. 2 (filled red symbols) and they are consistent with the rate for the optical band predicted by our model (solid red line in Fig. 2). Also, no credible OA was found in the Faint Sky Variability Survey project (Vreeswijk 2002).

Present and future major surveys in the optical are shown in Table 2. Most of the optical survey parameters are obtained from Rau et al. (2009). In Table 2, we report the survey name (Col. 1), its field of view (FOV) and its cadence (Cols. 2 and 3). The limiting flux density and the coverage, representing the sky area covered per night, are reported in Cols. 3 and 4, respectively. Through Fig. 2 we can derive the rate $R_{\rm OA}$ of OAs that have their peak flux density above each survey limiting flux. This is reported in units of deg^{-2} yr^{-1} in Col. 7 of Table 2. Similarly, from Fig. 3 it is possible to estimate the average duration $\langle T \rangle$ of the OA above the survey limiting flux (Col. 8 in Table 2). In brackets, we indicate the upper and lower estimates of the average duration (i.e., corresponding to the 1σ error bars in Fig. 3). We derive the rate of OAs (expressed in number of OA per year, last column of Table 2) in a given survey as $N_{\rm OA} = R_{\rm OA} \times C \times \langle T \rangle$, where C is the fraction of the sky covered by the survey per night (coverage in Table 2)

4.2. X-ray surveys

Searching for GRB afterglows in X-ray surveys led to the discovery of few flare stars (Grindlay 1999; Greiner et al. 2000). The 27 X-ray transients, detected in the 5.5 year survey of Ariel V (Pye & McHardy 1983), provide a conservative upper limit of 1.15×10^{-3} deg^{-2} yr^{-1}, corresponding to a flux $\approx$0.06 mJy (Grindlay 1999). This is consistent with our predictions for the X-ray band (solid blue line in Fig. 2) at the same flux limit.

Among the widest X-ray surveys, the ROSAT All-Sky Survey covered the full sky reaching a limiting flux of 4×10^{-13} erg cm^{-2} s^{-1} (0.5–2 keV) in almost six months. This flux limit (assuming a spectrum with photon index –2) corresponds to a flux density of $\sim 4 \times 10^{-5}$ mJy which, according to our estimates, gives a rate $R_{\rm OA} \sim 8 \times 10^{-4}$ deg^{-2} yr^{-1}. The RASS scan procedure covered a full-sky circle of width 2 deg every orbit corresponding to $\sim$12 000 deg^2 day^{-1}. According to our estimates (Fig. 2 and Table 2), the typical duration of the OA above the RASS flux limit should be $\sim$ 1 day so that the expected OA number should be $\sim$4.8 during the six month lifetime of the survey. This result is consistent with the estimate of Greiner et al. (2000). They effectively searched in the RASS for GRB afterglows and concluded that of the 23 candidates only a few could be due to GRBs, finding that most of the others are flare stars. The second release of the RASS, 2RXS[2] has been extended to a flux limit a factor of 4 deeper than the first release. Therefore, we expect to have $\sim$12 OAs in the 2RXS.

In the X-ray band *Chandra* and *XMM-Newton* have performed deep surveys but, because of their small FOV, at the expense of a relatively small portion of the sky explored (see Brandt & Hasinger 2005). The observing strategy in these surveys was not a scanning mode as in the RASS, but rather the combination of pointed repeated observations of the same field. Therefore, it is difficult to reconstruct the overall sky coverage. As a gross estimate, we can compute the expected number of OAs by multiplying the predicted rate (according to our results of Fig. 2) times the area of the sky covered. We stress that this is an overestimate of the number of OAs that could be detected by these surveys. Among the deepest surveys, the 2 Ms *Chandra* Deep Field North covered 0.13 deg^2 in the 0.5–8.0 keV band down to a flux limit of $\sim 10^{-16}$ erg cm^{-2} s^{-1} (Alexander et al. 2003). To such a flux limit, we predict less than 10^{-2} OA yr^{-1}. Similar rates are expected in the *XMM-Newton* Large Scale Survey (Pierre et al. 2004) which, with a sensitivity of $\sim 5 \times 10^{-15}$ erg cm^{-2} s^{-1} (0.5–2 keV) and a 10 deg^2 of sky coverage, should detect at most 0.1 OA yr^{-1}. Both *Chandra* and *XMM-Newton* have performed several other surveys, however, despite larger sky coverage than those mentioned above, this was at the expense of their sensitivity (e.g., the *XMM-Newton* Bright Serendipitous Survey – Della Ceca et al. 2004). Therefore, according to our predictions, there does not seem like there is an opportunity to detect any orphan afterglow in current deep X-ray surveys[3].

4.3. Orphan afterglow distinguishing properties

The most important question to address is how to distinguish OAs from other transients when they are detected in large sky surveys. As shown in Fig. 3, OAs appear as daily transients in optical and X-ray surveys, given the typical flux limits of current and forthcoming surveys (see Table 2), and many other extragalactic sources have similar duration. They will show a decaying light curve with a temporal slope, which is that of typical GRB afterglows, i.e., $\propto t^{-\delta}$ with $\delta \sim 1$–2 but not uniquely characterising GRBs as a class. The lack of any associated high energy γ-ray counterpart will hamper their classification as orphan afterglows of GRBs. The success of a transient survey is that of classifying, after discovery, the detected transients and to this aim a dedicated follow-up program is fundamental.

A first method of assessing the OA nature of the transient is with a systematic optical photometric and spectroscopic follow up. The optical/X-ray light curves, especially if the OA that is detected is still quite bright and/or before its light-curve peak, can be a very useful tool for a preliminary source classification. Indeed, its shape and its decay power-law index should be different from those of SNe or blazars. In addition to the ground-based optical facilities, the future satellite SVOM

[2] http://xmm.esac.esa.int/external/xmm_science/workshops/2014symposium

[3] In the XMM/EPIC database, whose variability richness will be fully explored by the EXTraS project (De Luca et al. 2015), we do not expect orphan afterglows to be present.

Table 2. Transient surveys in the optical and X-ray bands.

Survey	FOV (deg^2)	Cadence	F_{lim} (mJy)	Coverage (deg^2 $night^{-1}$)	Lifetime days	R_{OA} (deg^{-2} yr^{-1})	$\langle T \rangle$ days	# OA yr^{-1}
PTF	7.8	1m–5d	1.17×10^{-2}	1000		1.5×10^{-3}	1[0.2–3.8]	1.5
ROTSE–II	3.4	1d	1.17×10^{-1}	450		5.2×10^{-4}	0.4[0.1–1.7]	0.1
CIDA–QUEST	5.4	2d–1yr	4.60×10^{-2}	276		8.0×10^{-4}	0.5[0.1–2.3]	0.1
Palomar–Quest	9.4	0.5h–1d	1.17×10^{-2}	500	2003–2008	1.5×10^{-3}	1[0.2–3.8]	0.8
SDSS–II SS	1.5	2d	2.68×10^{-3}	150	2005–2008	3.2×10^{-3}	1.6[0.4–6.3]	0.8
Catilina	2.5	10m–1yr	4.60×10^{-2}	1200		8.0×10^{-4}	0.6[0.1–2.4]	0.6
SLS	1.0	3d–5yr	5.60×10^{-4}	2	2003–2008	5.2×10^{-3}	2.8[0.8–11]	0.03
SkyMapper	5.7	0.2d–1yr	7.39×10^{-2}	1000	2009–...	6.4×10^{-4}	0.5[0.2–2.0]	0.3
Pan–STARRS1	7.0	3d	7.39×10^{-3}	6000	2009–...	2.0×10^{-3}	1[0.3–4.4]	12
LSST	9.6	3d	4.66×10^{-4}	3300	2022–...	5.1×10^{-3}	3[0.8–11]	50
Gaia	0.5×2	20d	3.00×10^{-2}	2000	2014–2019	10^{-3}	1[0.5–5]	2
ZTF *	42.0	1d	2.00×10^{-2}	22 500	2017–...	1.1×10^{-3}	0.8[0.4–4.8]	20
RASS	3.1	...	4.00×10^{-5}	12 000	6 months	8.0×10^{-4}	1[0.3–4.4]	10
eROSITA	0.8	6 months	2.00×10^{-6}	4320*	4 years	3.0×10^{-3}	2[0.5–6.5]	26

Notes. Ongoing and future surveys are marked in boldface. Parameters of the optical surveys, field of view (FOV), cadence, limiting flux F_{lim}, coverage and lifetime are from the compilation of Rau et al. (2009). The rate of orphan afterglow R_{OA} above the survey limiting flux is obtained through the flux density distribution reported in Fig. 2. The average OA duration above this flux limit $\langle T \rangle$ is derived from Fig. 3 and from the parameters of the linear fits reported in Table 1 (minimum and maximum durations are shown in brackets). The last column shows the number of OAs per year detectable by the reported surveys. For the X-ray the sky coverage is intended for 24 h. (*) See `http://www.ptf.caltech.edu/ztf` and Bellm (2014).

(Basa et al. 2008), to be operational at the same epoch of LSST, will be able to perform simultaneous X-ray and optical observations of OA candidates.

A final identification is given by optical spectroscopy. The spectral continuum and the absorption lines present in the optical-near-IR (NIR) spectra of the afterglow are very different from those typically found in SNe or blazars (Fynbo et al. 2009; Christensen et al. 2011). Nonetheless, spectra with a sufficient signal-to-noise ratio are needed. To date this requirement is fulfilled down to $R \sim 22$ with a reasonable amount of integration time (~2 h) (e.g., with X-Shooter at ESO/VLT). Future larger telescopes will also make possible to obtain similar results for fainter objects. Therefore, with the possible increase of transient detections from future surveys, a considerable amount of telescope time may be necessary for a systematic optical follow up of unknown transients and of potential OA candidates. Among projects that could substantially contribute to the broadband (optical to NIR) spectroscopy of transients discovered in surveys there is the Son Of X-Shooter (SOXS; P.I. Campana), which has been proposed for the NTT with a considerable number of dedicated nights per year, as well as the Nordic Optical Telescope Transient Explorer (NTE)[4]. Another way to discriminate between OAs and other transients comes from the analysis of the broad spectral energy distribution (SED). Here we compare the typical SED of OAs with that of potential competitors extragalactic sources like SNe and blazars.

Since the most promising detections will be with the forthcoming LSST (Ivezic et al. 2008 – see Table 2), we only consider the OAs that will be detected by this survey. We predict a rate ~50 OAs per year. The overall SED (i.e., the convolution of the SEDs of all OAs detectable by the LSST survey) is shown by the hatched pink region in Fig. 4. The typical SED of OAs detectable by LSST peaks in the 10^{11-13} Hz range. The spectrum below the peak, in the GHz down to the MHz range scales $\propto \nu^2$.

Possible extragalactic variable sources that could compete with GRB orphan afterglows in brightness, frequency of discovery, and timescales are supernovae and blazars. Figure 4 shows the SED of two blazars: the Flat Spectrum Radio Quasar (FSRQ) 3C454.3 and BLLac itself as representative of the respective classes (see Ghisellini et al. 2010). Two supernovae are also shown: SN 1978K as a possible representative of highly luminous supernovae and the GRB980425/SN1998bw (Galama et al. 1998) for the class of associated GRB–SNe. For all these sources, we report their SED as obtained by multifrequency observational campaigns and retrieved from Italian Space Agency (ASI) Science Data Center Sed Builder tool[5]. The solid curves in Fig. 4 are not physical models, and only illustrative of the overall broadband SED of these classes of objects. For the blazars, we also show what their SED would be like if they were shifted at $z = 2$, i.e., at the typical distance of long GRBs.

For comparison, in Fig. 4 we show the LSST flux limit (red square symbol). The OAs that LSST can detected when their jet emission is fully visible by the off-axis observer already have their peak frequency below the optical band, in the mm region. This is because the peak of the OA emission is reached several months after the burst (Sect. 3 – see also G14). Furthermore, Figure 4 shows that their emission in the MHz/GHz region is still in the self-absorbed regime. In contrast, BLLacs and SN emission like 1998bw or 1978 K are characterized by a softer spectrum in the radio band than the typical OA detected in an optical survey like the LSST. Therefore, the follow up of these transients in the mm and GHz bands will characterize their different SED.

5. Discussion

Among previous works in the literature, which estimated the detection rate of OAs, Totani & Panaitescu (2002) considered 10 GRB of the pre-*Swift* era with well-monitored afterglow light curves as templates. By assuming different off-axis viewing angles, they estimated the rate of OAs in the X-ray, optical, and radio band. Their predictions were based on a very small number

[4] `http://dark.nbi.ku.dk/news/2014/nte_is_a_go/`

[5] `http://tools.asdc.asi.it`

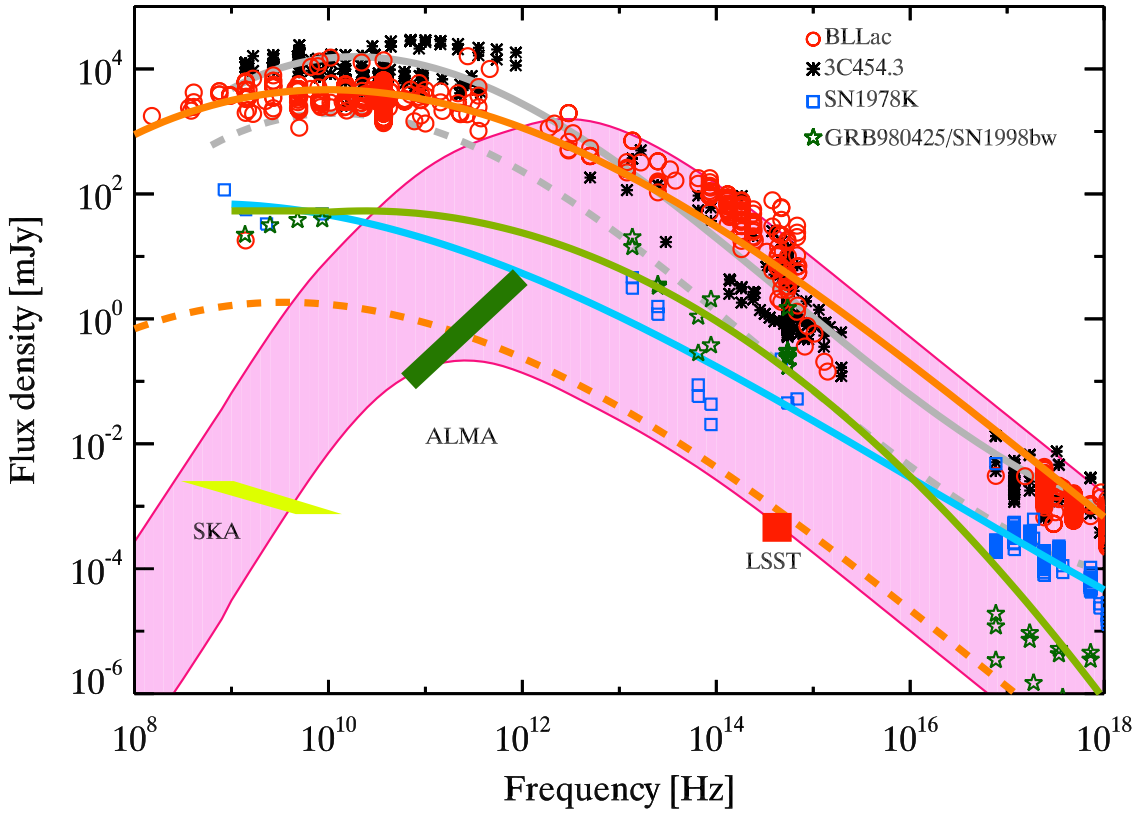

Fig. 4. Spectral energy distribution of the OAs that can be detected by the LSST (pink filled region). The SED of the low-power blazar BLLac (open circles), the FSRQ 3C 454.3 (asterisks), and of two supernovae, SN1978K (open squares) and the GRB–SN associated GRB980425/SN1998bw (open stars), are shown with different symbols. The solid lines provide an interpolation of the data points and do not represent any physical model. For the two blazars, we also show, with a dashed gray line for 3C 454.3 and dashed orange line for BLLac, how their spectra would appear if they were at $z = 2$ (typical of GRBs). The (5σ) limits for a 12 h continuum observation with the SKA is shown by the yellow shaded region. The green shaded region marks the limiting flux of an ALMA observation (32 antennas of 12 m for 3 h of observation in dual mode, from `https://almascience.eso.org/proposing/sensitivity-calculator`). The LSST limiting flux (see Table 2) is shown by the red square symbol.

of afterglows mostly representative of the bright afterglow population of GRBs. Similarly, Zou et al. (2007) adopt a set of fixed physical parameters (kinetic energy and micro-physical parameters) and only allow for a possible distribution of $\theta_{\rm jet}$. They predict a rate of 1.3×10^{-2} deg^{-2} yr^{-1} for OAs brighter than $R = 20$, which is consistent with our findings at the corresponding flux (red solid curve in Fig. 2). However, their flux distributions appear steeper than our model at low fluxes, thus predicting a higher rate of OAs in surveys that go deeper than the above limit. We consider that our estimates better represent the low flux end of the OA distribution since our code is calibrated with the entire GRB prompt emission flux distribution and includes a more representative sample of afterglows to fix the micro-physical parameters.

What is new in our model is that we predict the properties of OAs based on the observed properties of GRBs in the γ-ray band, considering as constraints the flux and fluence distribution of the population of GRBs detected by *Swift*, BATSE, and *Fermi*. Since the γ-ray energy detected in the prompt emission is a proxy of the kinetic energy driving the afterglow deceleration, our simulated population of bursts includes both high and low kinetic power bursts. The choice to reproduce the afterglow flux distribution of the complete BAT6 sample of *Swift* bursts, despite being composed by relatively bright events, ensures that we are extending the flux distribution of the synthetic GRB population to the low end better than what could be done with the limited number of GRBs detected in the pre-*Swift* era.

We have assumed that GRBs have a jet with a top-hat uniform structure, i.e., the kinetic energy and the bulk Lorentz factor are constant within the jet opening angle. Alternatively, (Rossi et al. 2002; Zhang & Mészáros 2002) GRB jets could be structured, i.e., the kinetic energy (and possibly also) the bulk Lorentz factor depend (as a power-law or exponentially) on the angle from the jet axis. In the former scenario considered in this work, orphan afterglows are naturally expected to dominate the number of GRBs in the Universe (considering a typical jet opening angle of few degrees). Even if the top-hat uniform jet emission can be seen when $\theta_{\rm view} \geq \theta_{\rm jet}$, its flux decreases drastically for off-axis observers, justifying the approximation that we can only see prompt emission from GRBs whose uniform jet is pointed toward the Earth (i.e., when $\theta_{\rm view} \leq \theta_{\rm jet}$). In the structured jet model, instead, there is always a portion of the jet that is pointing toward the observer. Therefore, the observed GRB properties only depend on the viewing angle $\theta_{\rm view}$ such that orphan afterglows should not exist in principle, since jet emission can be seen even at large angles from the jet (Salafia et al. 2015). However, also in this scenario OAs could still be present if either the prompt emission at large angles is below any detector threshold or if the jet is uniform within a relatively narrow core and highly structured (i.e., with a steeply decreasing energy profile) outside it, as suggested by recent results from the modeling of the luminosity function (Pescalli et al. 2015). In this model, the detection rates of OA would, at any rate, be lower than in the top-hat model adopted here as shown in Rossi et al. (2008).

Finally, note that in Fig. 1 we demonstrated that our afterglow model does not reproduce the X-ray early flux observed in the BAT6 sample of GRBs. This is because at early times the X-ray emission has been shown to be inconsistent with (i.e., larger than) the forward external shock model (e.g. Ghisellini et al. 2009). However, we used the afterglow emission of the population of OAs (as shown in Fig. 2) to predict the rate of detection of OAs by forthcoming X-ray surveys. Indeed, the time when the brightest OA peak in the X-ray (i.e., those that will likely be above the threshold of forthcoming X-ray surveys) is a few days after the prompt emission, i.e., when the emission also turns out to be dominated by the afterglow component in the X-ray (Ghisellini et al. 2009; D'Avanzo et al. 2012).

6. Conclusions

We computed the emission properties of the population of orphan afterglows in the optical and X-ray band. Our simulation procedure relies on what we have so far observed for a well-defined and complete sample of GRBs detected by *Swift* (Salvaterra et al. 2012) for which the X-ray, optical, and radio emission have been extensively studied (Campana et al. 2012; D'Avanzo et al. 2012; Covino et al. 2013; Melandri et al. 2014; Ghirlanda et al. 2013b).

Our model allows us to predict the expected rate of detection of OAs in past, current, and future optical and X-ray surveys (Table 2). For a similar work in the radio band, see Ghirlanda et al. (2014; see also Metzger et al. 2015). Most past and ongoing optical surveys have a small chance of of detecting OAs. Among these, the Palomar Transient Factory (PTF; Law et al. 2009) could marginally see one OA per year (consistent with Rau et al. 2009, predictions) given its relatively low sensitivity compensated by the large portion of the sky covered per night (10^3 deg^2). Instead, according to our model, an optical survey like that of Pan-STARRS1, which will cover 6000 deg^2 per night could already detect a dozen of OAs per year. Higher detection rates are expected for the forthcoming development of the PTF survey. The Zwicky Transient Facility (Bellm 2014), which is designed specifically for transients discovery, will cover about 22 500 deg^{-2} per night down to a limiting magnitude ∼20.5. We expect that it will detect ∼20 OA yr^{-1}. A considerably larger number of OAs will be accessible with the Large Synoptic Sky Telescope survey (LSST; Ivezic et al. 2008). The telescope will have a 9.6 deg^2 FOV and will be able to survey 10^4 deg^2 of the sky every three nights down to a limiting magnitude for point sources $R \sim 24.5$. With these parameters, we estimate it could detect 50 OA yr^{-1}.

An interesting prediction concerns the *Gaia* satellite (Lindegren 2010). It will carry two telescopes each one with a FOV of $0.7° \times 0.7°$ and will scan an angle of 360° every six hours. Therefore, it will cover ∼2000 deg^2 per day performing a survey down to a limiting flux of 0.03 mJy. According to our model, $R_{\rm OA} \sim 10^{-3}$ deg^{-2} yr^{-1} at this flux limit so that we predict that *Gaia* will detect about 10−15 OAs in its 5 year mission. This estimate is consistent with that reported in Japelj & Gomboc (2011). Given the depth of forthcoming optical surveys, we expect that OAs will have a typical redshift $z \sim 2$. At these distances, the typical GRB host galaxy should be fainter than the LSST limiting magnitude (Hjorth et al. 2012).

The difficulty will be to disentangle these OAs from other (galactic and extragalactic) transients that will be detected with similar flux and temporal behavior. The follow up in the optical and X-ray will secure the sampling of the light curve which could be the first hint to the OA nature (with respect to potential other extragalactic transients like supernovae and blazars). The availability of dedicated facilities or assigned observing time at different ground-based facilities will be crucial in this respect. Optical/NIR spectroscopy will discriminate extragalactic transients (e.g. Gorosabel et al. 2002), low-frequency (mm and radio bands) observations[6] could be used (as shown in Fig. 4) to distinguish among possible competing transients sources. For particularly low-redshift transients, the search for the host galaxy could also provide further clues as to their nature.

Here we computed the OA flux cumulative distribution at the reference frequency of 443 GHz, which is one of the frequencies covered by, e.g., ALMA. We verified that the few hundred GHz range is where OAs are brightest considering the typical timescales when they become visible (Sect. 2). Indeed, at 40 GHz and 4000 GHz the flux cumulative curves in Fig. 2 lie below the solid green curve representing the flux density at 443 GHz. The *Herschel*/SPIRE survey ATLAS[7], one of the widest covering a total of 500 deg^2, is limited by the confusion limit of 5−7 mJy at 250−500 μm so that we expect less than 0.1 OA yr^{-1}. *Spitzer* SWIRE[8] observed six fields in the northern and southern sky with typical areas between ∼4.2 deg^2 and ∼12 deg^2 with higher sensitivities of few tens of μJy in the low-frequency channels (IRAC) at 3.6 μm and 4.5 μm. These fields were covered on different timescales between one and six days. According to our model we expect a rate of less than one OA per year in such fields above the deepest flux limits of this survey.

Among forthcoming X-ray surveys, we consider the extended ROentgen Survey with the Imaging Telescope Array (eROSITA – Merloni et al. 2012), which will cover the full sky up to 10 keV with a flux limit $\sim 2 \times 10^{-14}$ erg^{-1} cm^{-2} s^{-1} in the 0.5−2 keV band. Therefore, $\sim 3 \times 10^{-3}$ deg^{-2} yr^{-1} OA should be reachable by this survey (Table 2). According to the planned scanning strategy, a full circle of width 2 degree will be covered every four hours. This corresponds to ∼4320 deg^2 day^{-1}. The expected OA number is ∼26 yr^{-1} (but see also Khabibullin et al. 2012). A larger number of OAs (by a factor 2) could be reached by the WFXT survey (e.g. Rosati et al. 2011).

Acknowledgements. ASI I/004/11/0 and the 2011 PRIN-INAF grant are acknowledged for financial support. S. Covino, G. Ghisellini, and L. Nava are acknowledged for stimulating discussions. Development of the Boxfit code (van Eerten et al. 2012) was supported in part by NASA through grant NNX10AF62G issued through the Astrophysics Theory Program and by the NSF through grant AST-1009863. D.B. is funded through ARC grant DP110102034. We acknowledge the anonymous referee for useful comments that helped us to improve the manuscript.

References

Alexander, D. M., Bauer, F. E., Brandt, W. N., et al. 2003, AJ, 126, 539
Bannister, K. W., Murphy, T., Gaensler, B. M., Hunstead, R. W., & Chatterjee, S. 2011, MNRAS, 418, 2813
Basa, S., Wei, J., Paul, J., Zhang, S. N., & Svom Collaboration. 2008, in SF2A-2008, eds. C. Charbonnel, F. Combes, & R. Samadi, 161
Becker, A. C., Wittman, D. M., Boeshaar, P. C., et al. 2004, ApJ, 611, 418
Bell, M. E., Fender, R. P., Swinbank, J., et al. 2011, MNRAS, 415, 2
Bellm, E. 2014, in The Third Hot-wiring the Transient Universe Workshop, eds. P. R. Wozniak, M. J. Graham, A. A. Mahabal, & R. Seaman, 27

[6] The LSST will start operating approximately in the same period as the Square Kilometer Array (SKA).
[7] http://www.h-atlas.org/ http://www.h-atlas.org/survey/fields
[8] http://swire.ipac.caltech.edu/swire/astronomers/program.html http://swire.ipac.caltech.edu/swire/public/faqs.html#where

Blandford, R. D., & McKee, C. F. 1976, Physics of Fluids, 19, 1130
Bower, G. C., & Saul, D. 2011, ApJ, 728, L14
Brandt, W. N., & Hasinger, G. 2005, ARA&A, 43, 827
Campana, S., Salvaterra, R., Melandri, A., et al. 2012, MNRAS, 421, 1697
Carilli, C. L., Ivison, R. J., & Frail, D. A. 2003, ApJ, 590, 192
Christensen, L., Fynbo, J. P. U., Prochaska, J. X., et al. 2011, ApJ, 727, 73
Costa, E., Frontera, F., Heise, J., et al. 1997, Nature, 387, 783
Covino, S., Melandri, A., Salvaterra, R., et al. 2013, MNRAS, 432, 1231
Croft, S., Bower, G. C., Ackermann, R., et al. 2010, ApJ, 719, 45
D'Avanzo, P., Salvaterra, R., Sbarufatti, B., et al. 2012, MNRAS, 425, 506
De Luca, A., Salvaterra, R., Tiengo, A., et al. 2015, ArXiv e-prints [arXiv:1503.01497]
Della Ceca, R., Maccacaro, T., Caccianiga, A., et al. 2004, A&A, 428, 383
Frail, D. A., Kulkarni, S. R., Sari, R., et al. 2001, ApJ, 562, L55
Frail, D. A., Kulkarni, S. R., Ofek, E. O., Bower, G. C., & Nakar, E. 2012, ApJ, 747, 70
Fynbo, J. P. U., Jakobsson, P., Prochaska, J. X., et al. 2009, ApJS, 185, 526
Galama, T. J., Vreeswijk, P. M., van Paradijs, J., et al. 1998, Nature, 395, 670
Gal-Yam, A., Ofek, E. O., Poznanski, D., et al. 2006, ApJ, 639, 331
Gehrels, N., Ramirez-Ruiz, E., & Fox, D. B. 2009, ARA&A, 47, 567
Ghisellini, G., Nardini, M., Ghirlanda, G., & Celotti, A. 2009, MNRAS, 393, 253
Ghisellini, G., Tavecchio, F., Foschini, L., et al. 2010, MNRAS, 402, 497
Ghirlanda, G., Nava, L., Ghisellini, G., et al. 2012, MNRAS, 420, 483
Ghirlanda, G., Ghisellini, G., Salvaterra, R., et al. 2013a, MNRAS, 428, 1410
Ghirlanda, G., Salvaterra, R., Burlon, D., et al. 2013b, MNRAS, 435, 2543
Ghirlanda, G., Burlon, D., Ghisellini, G., et al. 2014, PASA, 31, 22
Gorosabel, J., Fynbo, J. U., Hjorth, J., et al. 2002, A&A, 384, 11
Greiner, J., Hartmann, D. H., Voges, W., et al. 2000, A&A, 353, 998
Grindlay, J. E. 1999, ApJ, 510, 710
Hjorth, J., Malesani, D., Jakobsson, P., et al. 2012, ApJ, 756, 187
Hopkins, A. M., & Beacom, J. F. 2008, ApJ, 682, 1486
Ivezic, Z., Tyson, J. A., Abel, B., et al. 2008, ArXiv e-prints [arXiv:0805.2366]
Japelj, J., & Gomboc, A. 2011, PASP, 123, 1034
Khabibullin, I., Sazonov, S., & Sunyaev, R. 2012, MNRAS, 426, 1819
Law, N. M., Kulkarni, S. R., Dekany, R. G., et al. 2009, PASP, 121, 1395
Lazio, T. J. W., Clarke, T. E., Lane, W. M., et al. 2010, AJ, 140, 1995
Levinson, A., Ofek, E. O., Waxman, E., & Gal-Yam, A. 2002, ApJ, 576, 923
Liang, E.-W., Yi, S.-X., Zhang, J., et al. 2010, ApJ, 725, 2209
Lindegren, L. 2010, IAU Symp., eds. S. A. Klioner, P. K. Seidelmann, & M. H. Soffel, 261, 296
Malacrino, F., Atteia, J.-L., Boër, M., et al. 2007, A&A, 464, L29
Matsumura, N., Niinuma, K., Kuniyoshi, M., et al. 2009, AJ, 138, 787
Melandri, A., Covino, S., Rogantini, D., et al. 2014, A&A, 565, A72
Metzger, B. D., Williams, P. K. G., & Berger, E. 2015, ArXiv e-prints [arXiv:1502.01350]
Molinari, E., Vergani, S. D., Malesani, D., et al. 2007, A&A, 469, L13
Nakar, E., Piran, T., & Granot, J. 2002, ApJ, 579, 699
Nava, L., Salvaterra, R., Ghirlanda, G., et al. 2012, MNRAS, 421, 1256
Panaitescu, A., & Kumar, P. 2000, ApJ, 543, 66
Perna, R., Lazzati, D., & Fiore, F. 2003, ApJ, 585, 775
Pescalli, A., Ghirlanda, G., Salafia, O. S., et al. 2015, MNRAS, 447, 1911
Pierre, M., Valtchanov, I., Altieri, B., et al. 2004, J. Cosmol. Astropart. Phys., 9, 11
Pye, J. P., & McHardy, I. M. 1983, MNRAS, 205, 875
Rau, A., Greiner, J., & Schwarz, R. 2006, A&A, 449, 79
Rau, A., Schwarz, R., Kulkarni, S. R., et al. 2007, ApJ, 664, 474
Rau, A., Kulkarni, S. R., Law, N. M., & Bloom, J. S. 2009, PASP, 121, 1334
Rhoads, J. E. 1999, ApJ, 525, 737
Rossi, E., Lazzati, D., & Rees, M. J. 2002, MNRAS, 332, 945
Rossi, E. M., Perna, R., & Daigne, F. 2008, MNRAS, 390, 675
Rykoff, E. S., Aharonian, F., Akerlof, C. W., et al. 2005, ApJ, 631, 1032
Salafia, O. S., Ghisellini, G., Pescalli, A., Ghirlanda, G., & Nappo, F. 2015, MNRAS, 450, 3549
Salvaterra, R., Campana, S., Vergani, S. D., et al. 2012, ApJ, 749, 68
Sari, R., & Piran, T. 1999, A&AS, 138, 537
Totani, T., & Panaitescu, A. 2002, ApJ, 576, 120
van Eerten, H. J., & MacFadyen, A. I. 2011, ApJ, 733, L37
van Eerten, H., van der Horst, A., & MacFadyen, A. 2012, ApJ, 749, 44
van Paradijs, J., Groot, P. J., Galama, T., et al. 1997, Nature, 386, 686
Vreeswijk, P. M. 2002, Ph.D. Thesis, University of Amsterdam
Zhang, B., & Mészáros, P. 2002, ApJ, 571, 876
Zou, Y. C., Wu, X. F., & Dai, Z. G. 2007, A&A, 461, 115